Gas adsorption in the topologically disordered Fe-BTC framework

SUPPLEMENTARY INFORMATION

Adam F. Sapnik,[1] Christopher W. Ashling,[1] Lauren K. Macreadie,[2,3] Seok J. Lee,[2] Timothy Johnson,[4] Shane G. Telfer[2] and Thomas D. Bennett[1]*

1. Department of Materials Science and Metallurgy, University of Cambridge, Cambridge, CB3 0FS, United Kingdom.
2. MacDiarmid Institute for Advanced Materials and Nanotechnology, Institute of Fundamental Sciences, Massey University, Palmerston North, New Zealand.
3. School of Chemistry, University of Sydney, Sydney, NSW, 2006, Australia.
4. Johnson Matthey Technology Centre, Blount's Court, Sonning Common, RG4 9NH, United Kingdom.

* To whom correspondence should be addressed; E-mail: tdb35@cam.ac.uk

Table of Contents

Supplementary Methods

Surface Area Analysis

Brunauer–Emmett–Teller (BET) surface areas were calculated from N_2 adsorption isotherms at 77 K according to the following procedure.[1] The isotherm region where $v(1 - P/P_0)$ increases versus P/P_0, where v is the amount of N_2, was identified. Within this isotherm region, sequential data points that led to a positive intercept in the plot of $\frac{(P/P_0)}{v(1-P/P_0)}$ against P/P_0 were found. This plot yields a slope a and a positive intercept b. The BET surface area was then calculated according to the following equation:

$$A_{\text{BET}} = v_{\text{m}} \times \frac{1}{22400} \times \sigma_0 \times N_{\text{A}} \times 10^{-20}, \tag{1}$$

where N_{A} is Avogadro's constant and σ_0 is the cross-sectional area of a N_2 molecule, which is 16.2 Å^2.

Non-Local Density Functional Theory Analysis

Pore size distributions were extracted from the N_2 adsorption isotherms at 77 K using a non-local density functional theory (NL-DFT) approach.[2] Within NL-DFT, classical fluid density functional theory is used to construct adsorption isotherms in ideal pore geometries and then solve the adsorption integral equation. The main limitation of NL-DFT as applied here is the absence of a specific kernel designed for MOFs.[3] Instead, kernels for activated carbons are often used given the majority of accessible surface within a MOF is organic in nature – that is the 1,3,5-benznetricabolate anion in the case of MIL-100 and Fe-BTC.[4,5] Furthermore, while the use of NL-DFT methods on amorphous MOFs has proven valuable, it cannot be scrutinised with the same quantitative level of detail as for crystalline systems.[3] NL-DFT methods have also been reported to underestimate the pore dimensions, compared to the expected van der Waals dimensions.[6,7] Pore size distributions were calculated within the SAIEUS software employing a *carbon–N₂, 2D heterogenous* kernel and a regularisation parameter (λ) of 1.75.[8]

Virial Analysis

Isosteric heat of adsorption, Q_{st}, values were calculated from adsorption isotherms measured at 273 and 293 K for CO_2, CH_4 and C_3H_6.[9] The isotherms were fit *via* global optimisation to the virial equation:

$$\ln P = \ln N + \frac{1}{T} \sum_{i=0}^{m} a_i N^i + \sum_{i=0}^{m} b_i N^i, \tag{2}$$

where *P* is pressure, *N* is the amount of gas adsorbed, *a* and *b* are the virial coefficients, *m* and *n* are the number of coefficients required to model the isotherm. Q_{st} values were then derived using the parameters obtained from the virial fits using the following equation:

$$Q_{\text{st}} = -R \sum_{i=0}^{m} a_i N^i. \tag{3}$$

The heat of adsorption at near-zero coverage were approximated using the following equation:

$$Q_{\text{st}}^0 \approx -R \times a_0. \tag{4}$$

Ideal Adsorbed Solution Theory Analysis

Thermodynamic gas selectivities for equimolar mixtures of CO_2/N_2, CH_4/N_2 and CO_2/CH_4 at 273 K were calculated using ideal adsorbed solution theory (IAST) in the IAST++ software package.[10,11] The pure-component isotherms of CO_2, N_2 and CH_4 for both MIL-100 and Fe-BTC were first fit to either a dual-site Langmuir-Freundlich [Eq. 5], Langmuir-Freundlich [Eq. 6], dual-site Langmuir [Eq. 7] or Langmuir [Eq. 8] model:

DSLF
$$n(P) = q_1 \frac{(k_1 P)^{n_1}}{1 + (k_1 P)^{n_1}} + q_2 \frac{(k_2 P)^{n_2}}{1 + (k_2 P)^{n_2}} \tag{5}$$

LF
$$n(P) = q \frac{(kP)^n}{1 + (kP)^n} \tag{6}$$

DSL
$$n(P) = q_1 \frac{k_1 P}{1 + k_1 P} + q_2 \frac{k_2 P}{1 + k_2 P} \tag{7}$$

L
$$n(P) = q \frac{kP}{1 + kP} \tag{8}$$

$n(P)$ is the number of moles of gas adsorbed on the surface when in equilibrium with a pure gas phase as a function of its pressure P. These parameters were used afterwards to carry out IAST calculations. The selectivity, $S_{a/b}$, was calculated using the following equation:

$$S_{a/b} = \frac{X_a Y_b}{X_b Y_a} \tag{9}$$

X is the mole fraction in the adsorbed phase and Y is the mole fraction in the gas phase.
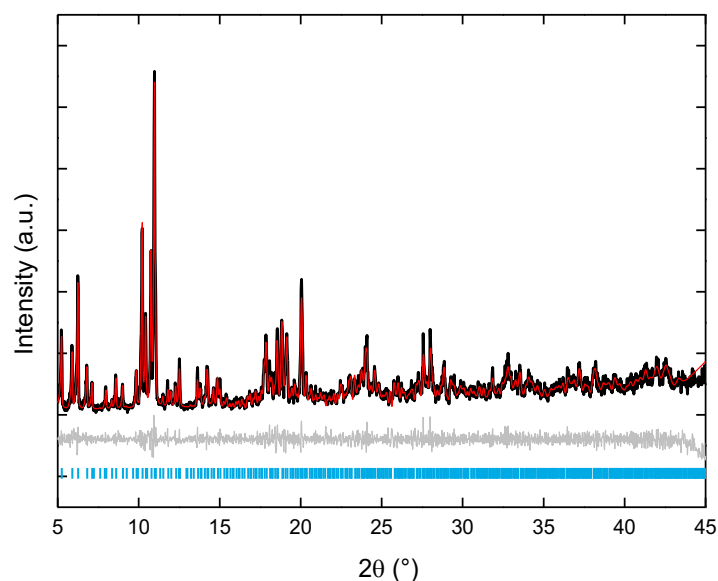
Pawley Refinement of MIL-100

Figure S1 Experimental data (black), calculated diffraction pattern (red), difference function (grey) and symmetry-allowed reflections (blue tick marks). Symmetry-allowed reflections were calculated from the reported crystallographic information file in Ref. 12. Data reproduced from Ref. 13.

Table S1 Crystallographic data from Pawley refinement of MIL-100.

R_{wp} = 9.48	Experimental	Reported [12]
$a = b = c$	73.25(3)	73.340(1)
$\alpha = \beta = \gamma$	90	90

BET Analysis Parameters – Nitrogen

Table S2 Refinement parameters obtained from BET analysis of N_2 adsorption isotherms at 77 K.

	MIL-100	Fe-BTC
Slope	0.00294	0.0636
Intercept	0.0000308	0.000260
Correlation coefficient	0.999711	0.999887
C constant	96.301	245.661
Surface area ($m^2\ g^{-1}$)	1465.627	68.170

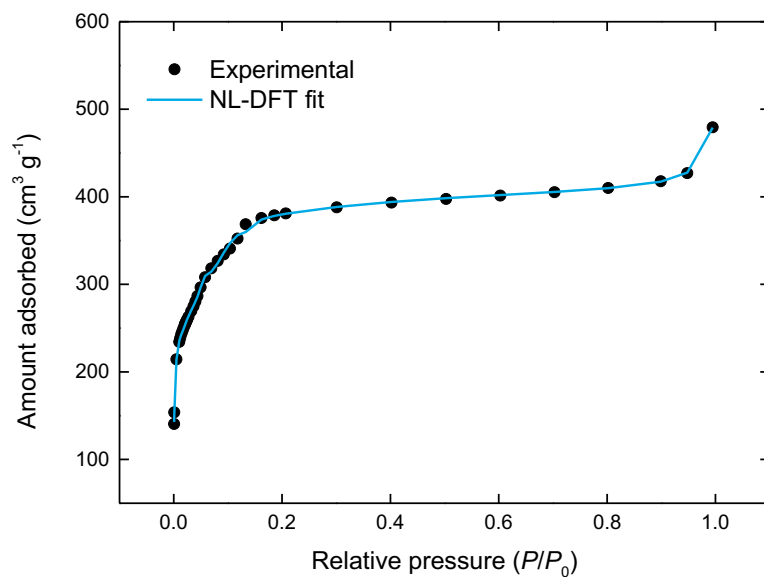# Non-Local Density Functional Theory Analysis

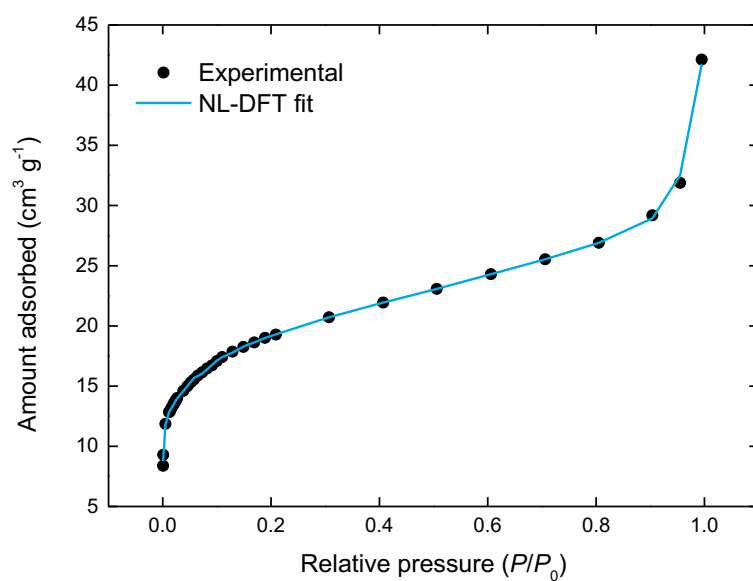**Figure S2** Experimental N$_2$ adsorption isotherm for MIL-100 (black circles) at 77 K and the NL-DFT fit (blue line).

Figure S3 Experimental N$_2$ adsorption isotherm for Fe-BTC (black circles) at 77 K and the NL-DFT fit (blue line).
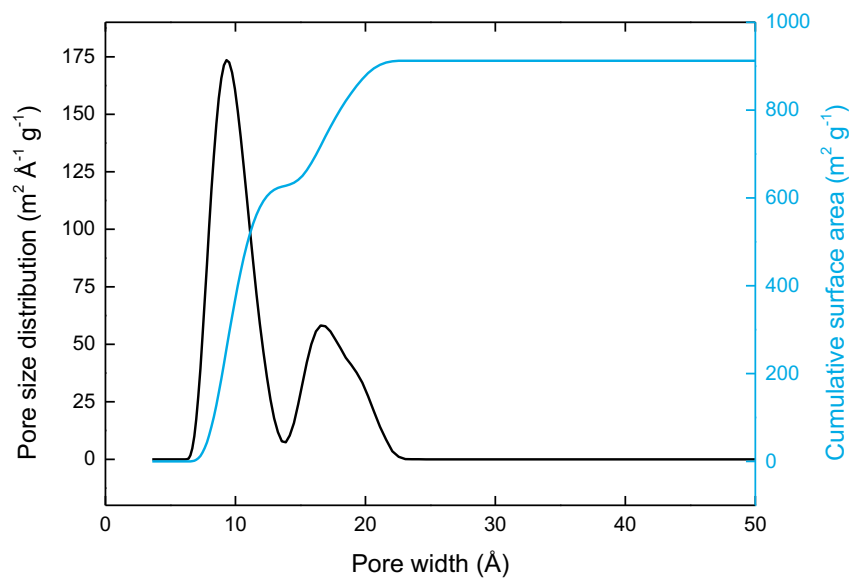
Pore Size Distributions

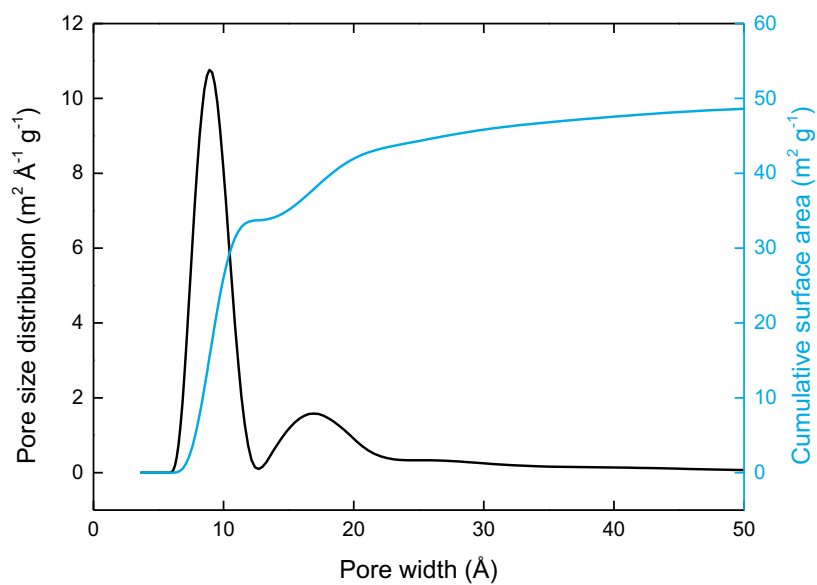**Figure S4** Pore size distribution (black) and cumulative surface area (blue) for MIL-100 from NL-DFT analysis.

Figure S5 Pore size distribution (black) and cumulative surface area (blue) for Fe-BTC from NL-DFT analysis.
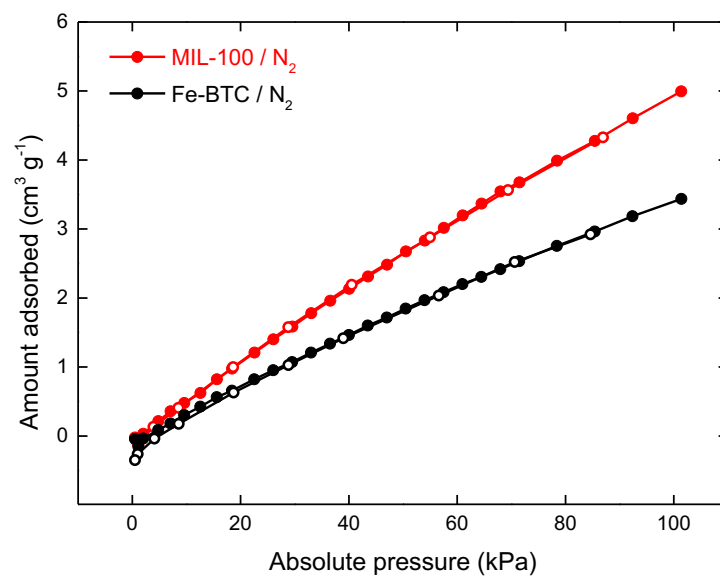
Nitrogen Isotherms

Figure S6 N_2 adsorption (closed) and desorption (open) isotherms at 273 K for MIL-100 (red) and Fe-BTC (black).

Adsorbate Properties

Table S3 Properties of the adsorbate molecules used in this study, values taken from Ref. 14.

	Molecular dimensions (Å)	Polarizability (×10²⁵ / cm³)	Dipole Moment (×10¹⁸ / esu cm)	Quadrupole moment (×10²⁶ /esu cm²)
N_2	3.64–3.80	17.403	0	1.52
Xe	4.047	40.44	0	0
Ar	3.542	16.411	0	0
H_2	2.827–2.89	8.042	0	0.662
CO_2	3.3	29.11	0	4.30
CH_4	3.758	25.93	0	0
C_2H_4	4.163	42.52	0	1.50
C_2H_6	4.443	44.3–44.7	0	0.65
C_3H_6	4.678	62.6	0.366	0
C_3H_8	4.30–5.118	62.9–63.7	0.084	0

BET Analysis Parameters – Carbon Dioxide

Table S4 Refinement parameters obtained from BET analysis of CO_2 adsorption isotherms at 273 K.

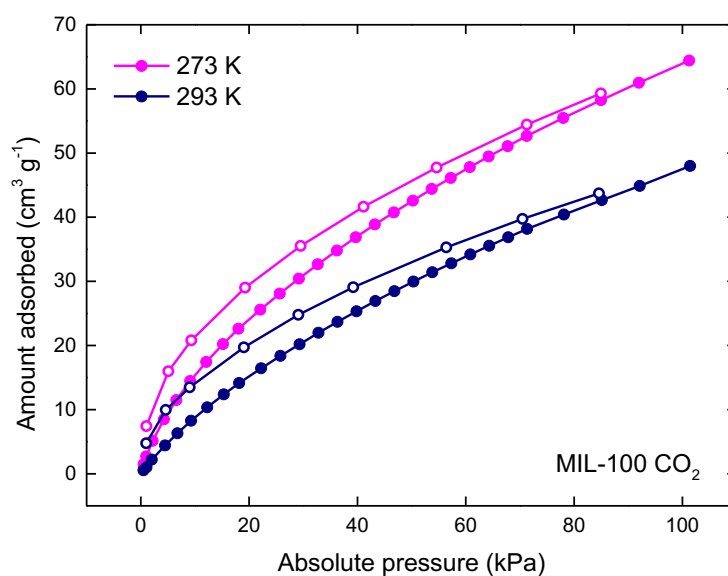|	**MIL-100**	**Fe-BTC**
Slope	0.0321	0.0545
Intercept	0.00391	0.00518
Correlation coefficient	0.999849	0.999621
C constant	9.210	11.508
Surface area (m^2 g^{-1})	126.725	76.585

Carbon Dioxide Isotherms

Figure S7 Adsorption (closed) and desorption (open) isotherms of CO_2 for MIL-100 at 273 (pink) and 293 K (navy).
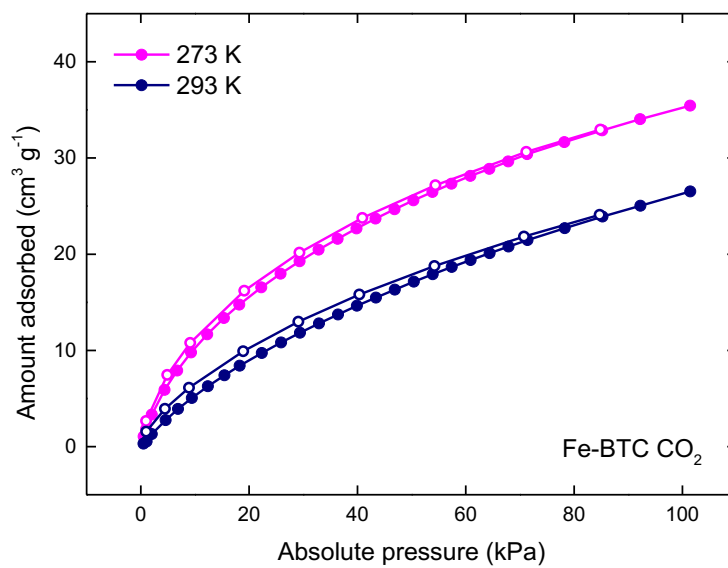
Figure S8 Adsorption (closed) and desorption (open) isotherms of CO_2 for Fe-BTC at 273 (pink) and 293 K (navy).
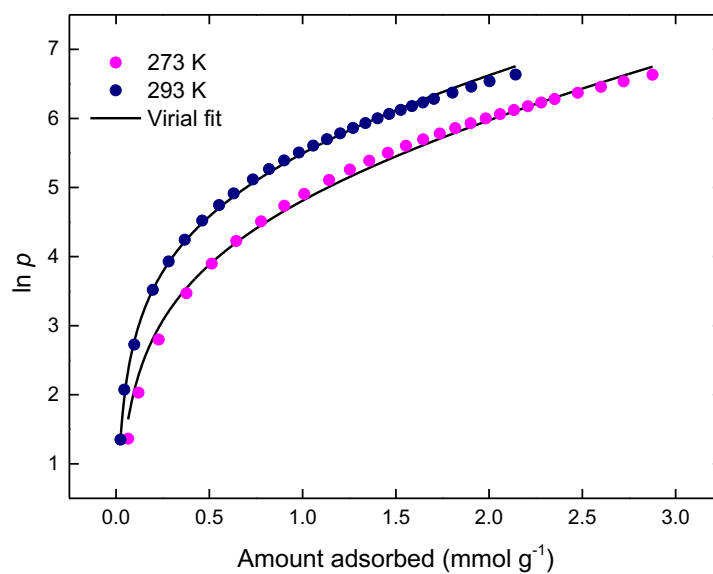
Carbon Dioxide Virial Fits

Figure S9 Virial fit (black lines) to the CO_2 adsorption data for MIL-100 at 273 (pink) and 298 K (navy).
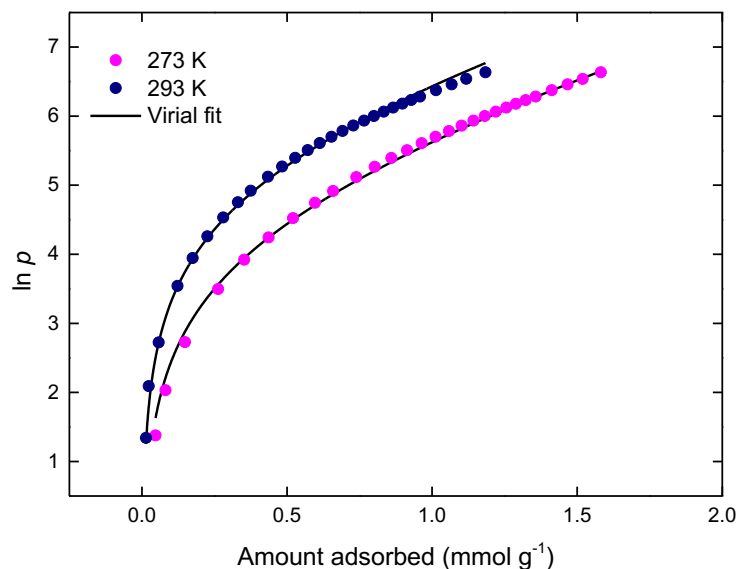
Figure S10 Virial fit (black lines) to the CO_2 adsorption data for Fe-BTC at 273 (pink) and 293 K (navy).

Table S5 Fitting parameters used for virial analysis of CO_2 in MIL-100 and Fe-BTC.

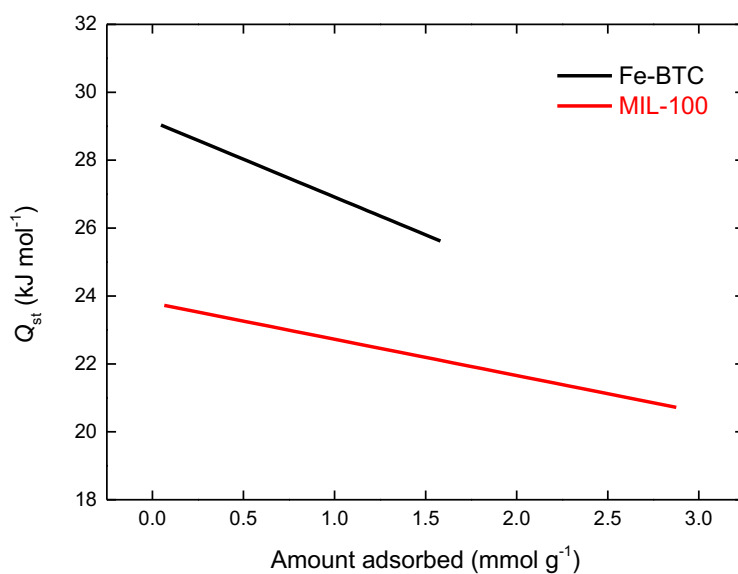|	**MIL-100**		**Fe-BTC**	
	Value	Uncertainty	Value	Uncertainty
a_0	-2861.97804	94.55277	-3504.88219	91.15603
a_1	128.50874	4.27335	267.70237	7.28523
b_0	14.82226	0.32837	17.47992	0.331527
R^2	0.9963		0.99672	
χ_v^2	0.00685		0.00607	

Carbon Dioxide Q_{st} Values

Figure S11 Q_{st} values for CO_2 for MIL-100 (red) and Fe-BTC (black) determined from the virial coefficients.
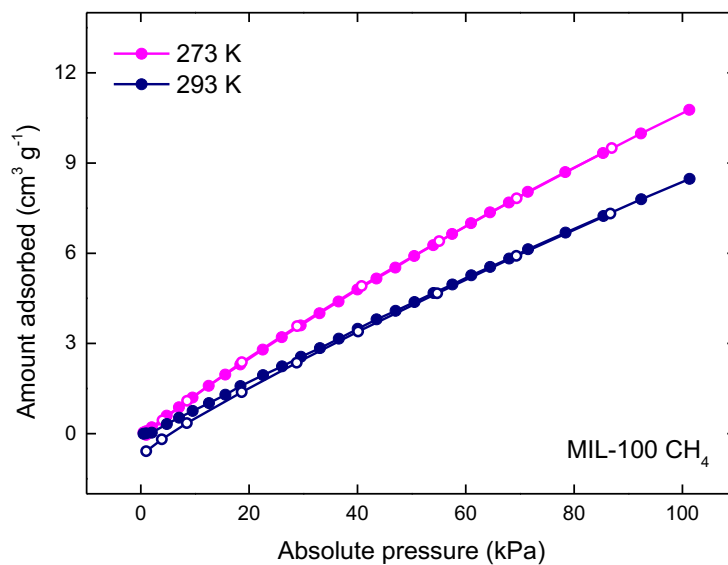
Methane Isotherms

Figure S12 Adsorption (closed) and desorption (open) isotherms of CH$_4$ for MIL-100 at 273 (pink) and 293 K (navy).
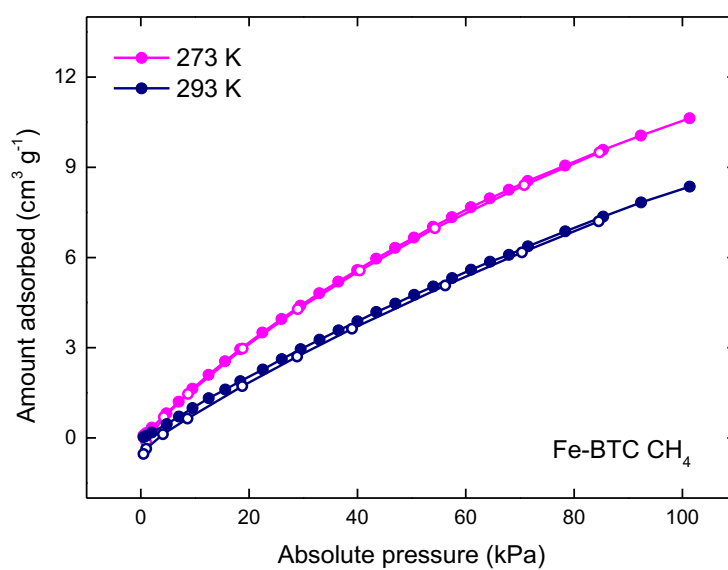

Figure S13 Adsorption (closed) and desorption (open) isotherms of CH$_4$ for Fe-BTC at 273 (pink) and 293 K (navy).
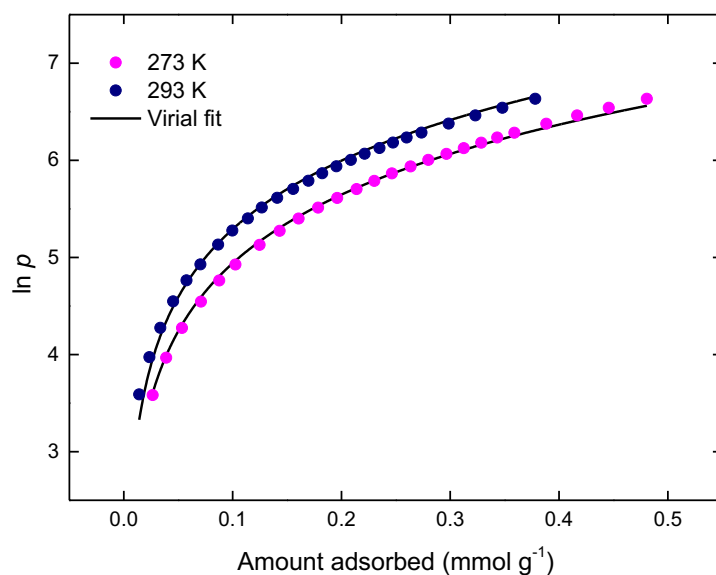
Methane Virial Fits

Figure S14 Virial fit (black lines) to the CH_4 adsorption data for MIL-100 at 273 (pink) and 293 K (navy).
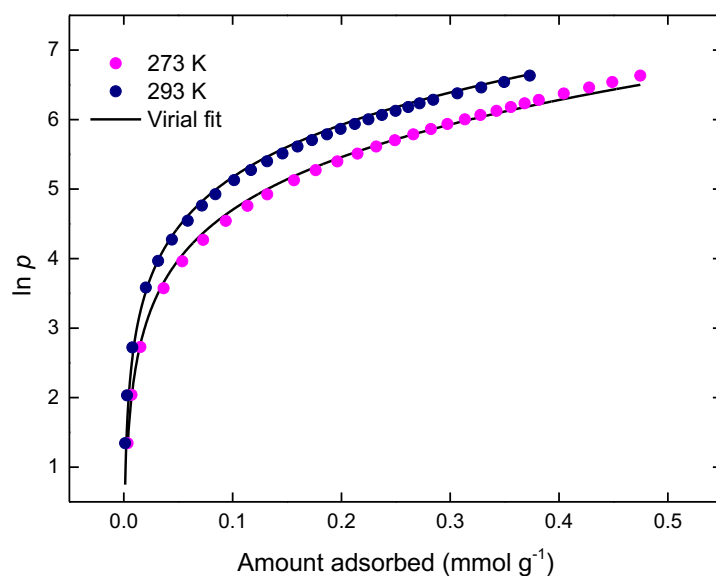

Figure S15 Virial fit (black lines) to the CH_4 adsorption data for Fe-BTC at 273 (pink) and 293 K (navy).

Table S6 Fitting parameters used for Virial analysis of CH_4 in MIL-100 and Fe-BTC. Note, the lowest pressure data (where there was minimal uptake) was excluded for MIL-100 to obtain a reasonable fit.

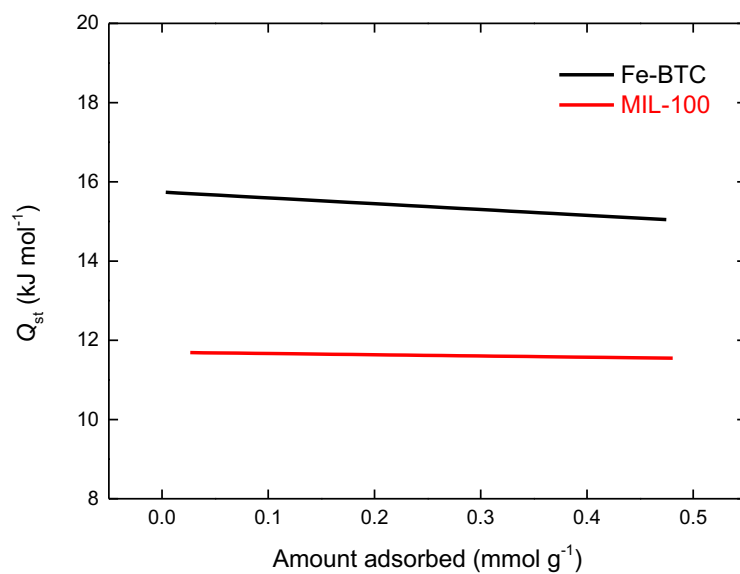|	MIL-100		Fe-BTC	
	Value	Uncertainty	Value	Uncertainty
a_0	-1406.90184	65.12101	-1893.30126	131.92175
a_1	37.29642	18.5466	176.35328	34.67179
b_0	12.38232	0.22695	13.87521	0.46047
R^2	0.99550		0.99247	
χ_v^2	0.00302		0.01393	

Methane Q_{st} Values

Figure S16 Q_{st} values for CH_4 for MIL-100 (red) and Fe-BTC (black) determined from the virial coefficients.
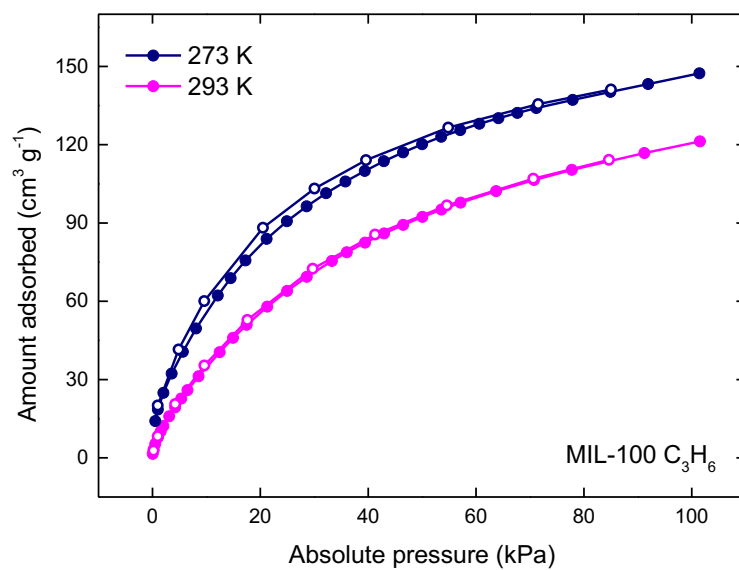
Propene Isotherms

Figure S17 Adsorption (closed) and desorption (open) isotherms of C_3H_6 for MIL-100 at 273 (navy) and 293 K (pink).

Figure S18 Adsorption (closed) and desorption (open) isotherms of C_3H_6 for Fe-BTC at 273 (navy) and 293 K (pink).

Propene Virial Fits

Figure S19 Virial fit (black lines) to the C_3H_6 adsorption data for MIL-100 at 273 (navy) and 293 K (pink).

Table S7 Fitting parameters used for Virial analysis of C_3H_6 in MIL-100.

	MIL-100	
	Value	Uncertainty
a_0	-4974.37325	251.30488
a_1	695.0499	75.96277
a_2	-57.30614	7.53744
a_3	4.7039	0.72963

b_0	19.75367	0.86481
b_1	-1.41067	0.24428
R^2	0.99585	
χ_v^2	0.00844	

Propene Q_{st} Values

Figure S20 Q_{st} values for C_3H_6 for MIL-100 determined from the virial coefficients.

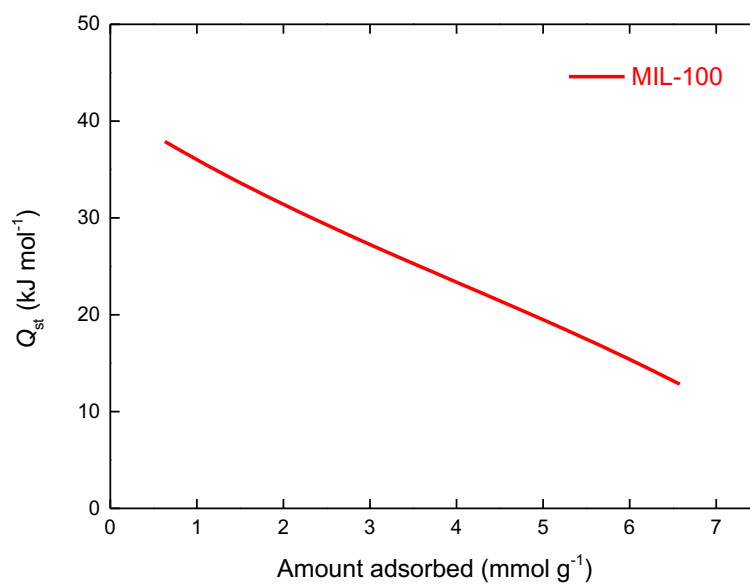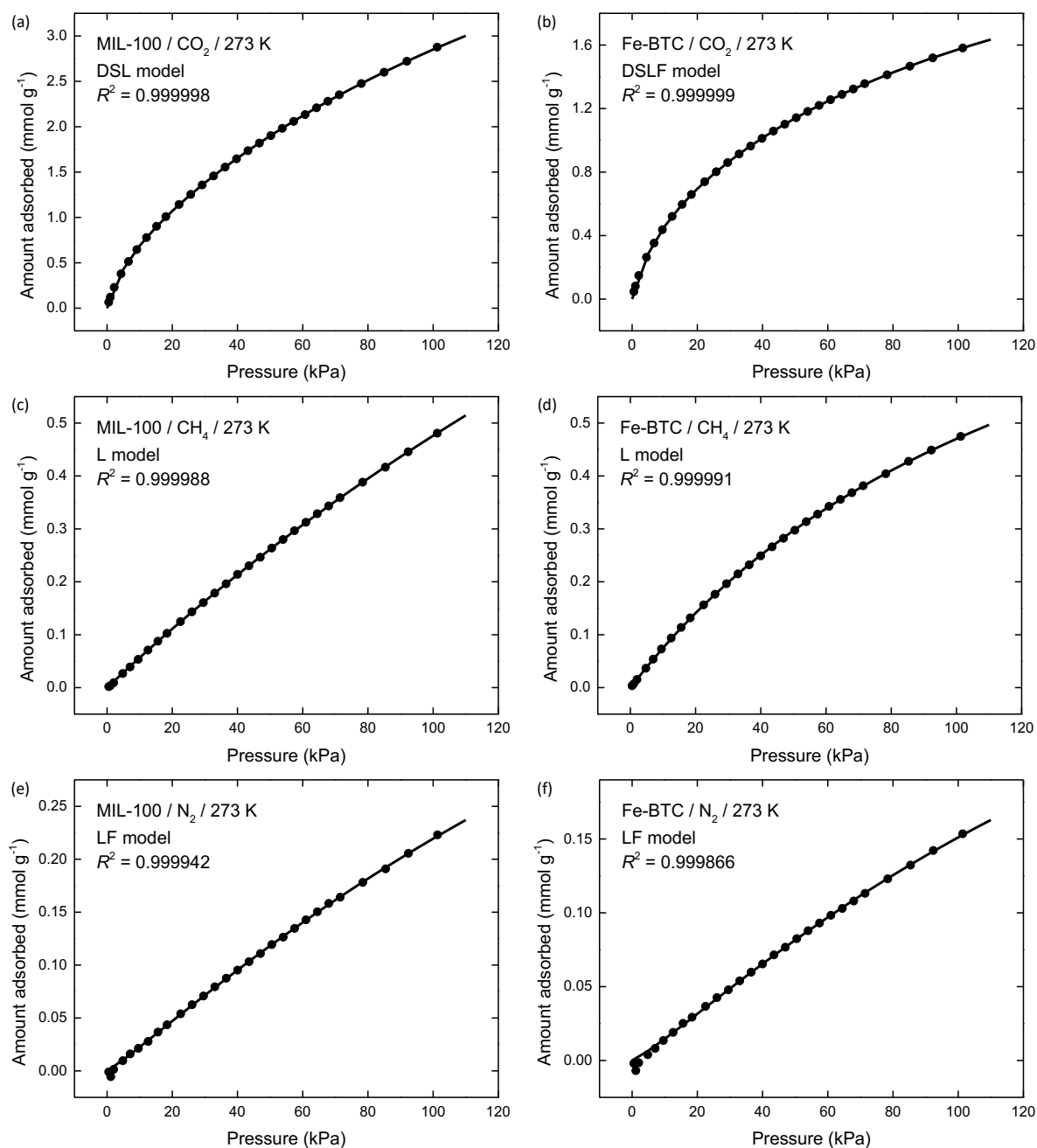# IAST Models

Figure S21 Experimental adsorption isotherms (black circle) and corresponding fit (black line) to either the Langmuir-Freundlich (LF), dual-site Langmuir (DSL), dual-site Langmuir Freundlich (DSLF) or Langmuir (L) model.

Table S8 Fitting parameters for the LF, DSL, DSLF and L models used to fit the experimental adsorption data for MIL-100 and Fe-BTC at 273 K

Fe-BTC / N_2 / LF	
q (mmol g^{-1})	0.485282
k (kPa^{-n})	0.00505054
n	1.16267
R^2	0.999866
MIL-100 / N_2 / LF	
q (mmol g^{-1})	0.855488
k (kPa^{-n})	0.00381855
n	1.1054
R^2	0.999942
MIL-100 / CO_2 / DSL	
q_1 (mmol g^{-1})	6.91921
q_2 (mmol g^{-1})	0.576341
k_1 (kPa^{-1})	0.00500354
k_2 (kPa^{-1})	0.163364
R^2	0.999998
Fe-BTC / CO_2 / DSLF	
q_1 (mmol g^{-1})	1.84866
q_2 (mmol g^{-1})	0.852406
k_1 (kPa^{-n1})	0.00862247
k_2 (kPa^{-n2})	0.074762
n_1	1.2241
n_2	0.896536
R^2	0.999999
MIL-100 / CH_4 / L	
q (mmol g^{-1})	2.66348
k (kPa^{-1})	0.00217646
R^2	0.999988
Fe-BTC / CH_4 / L	
q (mmol g^{-1})	1.13186
k (kPa^{-1})	0.00710647
R^2	0.999991

References

1   K. S. Walton and R. Q. Snurr, *J. Am. Chem. Soc.*, 2007, **129**, 8552–8556.
2   J. Jagiełło, *Langmuir*, 1994, **10**, 2778–2785.
3   G. Kupgan, T. P. Liyana-Arachchi and C. M. Colina, *Langmuir*, 2017, **33**, 11138–11145.
4   M. Rivera-Torrente, M. Filez, R. Hardian, E. Reynolds, B. Seoane, M. V. Coulet, F. E. Oropeza Palacio, J. P. Hofmann, R. A. Fischer, A. L. Goodwin, P. L. Llewellyn and B. M. Weckhuysen, *Chem. Eur. J.*, 2018, **24**, 7498–7506.
5   X. S. Wang, L. Li, J. Liang, Y. B. Huang and R. Cao, *ChemCatChem*, 2017, **9**, 971–979.
6   W. Li, Y. Zhang, C. Zhang, Q. Meng, Z. Xu, P. Su, Q. Li, C. Shen, Z. Fan, L. Qin and G. Zhang, *Nat. Commun.*, 2016, **7**, 1–9.
7   M. L. Ojeda, J. M. Esparza, A. Campero, S. Cordero, I. Kornhauser and F. Rojas, *Phys. Chem. Chem. Phys.*, 2003, **5**, 1859–1866.
8   Micromeritics, SAIEUS, version 3 (computer software), GA.
9   A. Nuhnen and C. Janiak, *Dalton Trans.*, 2020, **49**, 10295–10307.
10   A. L. Myers and J. M. Prausnitz, *A.I.Ch.E.*, 1965, **11**, 121–127.
11   S. Lee, J. H. Lee and J. Kim, *Korean J. Chem. Eng.*, 2018, **35**, 214–221.
12   P. Horcajada, S. Surblé, C. Serre, D. Y. Hong, Y. K. Seo, J. S. Chang, J. M. Grenèche, I. Margiolaki and G. Férey, *Chem. Commun.*, 2007, **100**, 2820–2822.
13   A. F. Sapnik, I. Bechis, S. M. Collins, D. N. Johnstone, G. Divitini, A. J. Smith, P. A. Chater, M. Addicoat, T. Johnson, D. A. Keen, K. E. Jelfs and T. D. Bennett, *Nat. Commun.*, 2021, **12**, 2062.
14   J. R. Li, R. J. Kuppler and H. C. Zhou, *Chem. Soc. Rev.*, 2009, **38**, 1477–1504.